

Impact of Helical Electromagnetic Fields on the Axion Window

Takeshi Kobayashi* and Rajeev Kumar Jain†

* *Kobayashi-Maskawa Institute for the Origin of Particles and the Universe,
Nagoya University, Nagoya 464-8602, Japan*

† *Department of Physics, Indian Institute of Science, Bangalore 560012, India*

E-mail: takeshi@kmi.nagoya-u.ac.jp, rkjain@iisc.ac.in

Primordial electromagnetic fields can strongly affect the cosmic evolution of axions, and vice versa. We show that if helical electromagnetic fields are coherently produced in the early universe, their remnants source a field velocity to the coupled axions and enhance the relic abundance of axion dark matter. We discuss the implications for the QCD axion and axion-like particles that are coupled to the SM or hidden gauge groups. For a QCD axion coupled to hidden photons, we find that the conventional window for the axion decay constant $10^8 \text{ GeV} \lesssim f \lesssim 10^{12} \text{ GeV}$ can be completely closed due to overproduction of axion dark matter by helical electromagnetic fields as little as $\alpha \Delta N_{\text{eff}} \gtrsim 10^{-12}$, where α is the gauge coupling and ΔN_{eff} is the effective extra relativistic degrees of freedom of the hidden photons.

Contents

1	Introduction	1
2	Axion Dynamics with Helical Electromagnetic Fields	2
2.1	Helical Electromagnetic Fields in the SM and Hidden Sector	3
2.2	Induced Axion Velocity	4
2.3	Backreaction from the Axion	6
2.4	Onset of Axion Oscillation	6
2.5	Numerical Example	7
3	Axion Relic Abundance	9
3.1	Constant-Mass Axion	9
3.2	QCD Axion	12
4	Conclusions and Discussion	15
A	Early Cosmological Evolution of Helical Electromagnetic Fields	17
A.1	Model with a Time-Dependent and Parity-Violating Background	17
A.2	Canonical Quantization	18
A.3	Redshifting of Electromagnetic Fields within Maxwell Theory	19

1 Introduction

Physics beyond the Standard Model (SM) can contain additional approximate global U(1) symmetries, that are spontaneously broken to yield pseudo-Nambu–Goldstone bosons (PNGBs). Perhaps the most famous example is the QCD axion [1, 2] arising from the breaking of the Peccei–Quinn U(1) symmetry [3] introduced for solving the strong CP problem. Low-energy effective field theories emerging from string theory also suggest the presence of axion-like particles [4–6]. Such PNGBs, which we collectively refer to as axions, are typically light and couple very weakly to normal matter, and thus provide a viable dark matter candidate.

The QCD axion obtains its mass through the coupling $\theta G\tilde{G}$ to the gluons. However in general, axions may possess couplings $\theta F\tilde{F}$ with other gauge fields either within the SM or in a hidden sector, Abelian or non-Abelian. Here, the product of the gauge field strength and its dual corresponds to a dot product of the electric and magnetic fields, i.e., $F\tilde{F} \propto E \cdot B$. This indicates that the dynamics of an axion can be modified in a background of helical electromagnetic fields.

Recently there is growing interest in the possibility that gauge fields were excited in the early universe. Cosmological production of the SM photon has long been a topic of study with the aim of explaining the origin of the galactic and intergalactic magnetic fields [7–9]. Nowadays, various kinds of gauge fields are also studied as a source of gravitational waves, as dark radiation, vector dark matter, in the context of anisotropic inflation, and so on. There is also a large literature on production mechanisms that spontaneously violate parity, in which case the resulting gauge particles can form helical electromagnetic fields; see e.g. [10–14]. Such a parity-odd gauge field background will, in turn, have a non-trivial effect on axions.

In this paper we analyze the dynamics of the QCD axion and axion-like fields in the presence of helical electromagnetic fields. If the helical fields are coherently excited in the early universe, it gives an effective linear potential to the axion via the coupling $\theta F\tilde{F}$, which forces the axion field to roll in one direction. We show that the $F\tilde{F}$ background has the net effect of increasing the relic abundance of axion dark matter, and therefore can completely transform the parameter window where axions are compatible with cosmology. Since an $E \cdot B$ composed of the SM photons vanishes in the reheating epoch as the conductivity of the universe rises and the electric fields short out, in this paper we will mainly focus on U(1) gauge fields in a hidden sector, and show that hidden electromagnetic fields can significantly modify the axion window. However, the SM electromagnetic fields can also have strong effects if the reheating temperature is sufficiently low.

Before proceeding with our analysis, we should remark that the possibility of helical fields affecting the axion dynamics was first pointed out in [15]. However this work studies the effect in a universe with vanishing electric fields and argues that the axion obtains a significant velocity by helical magnetic fields alone, even though in such a case there is no coherent $F\tilde{F}$ and so there should be no source for the axion velocity. We explicitly show that electric fields are necessary for affecting the axion dynamics, in disagreement with [15]. Similar conclusions on this point were reached in [16, 17], which studied helical SM magnetic fields in a conducting cosmological plasma (and hence with tiny electric fields) and found the effect on the QCD axion to be negligible. Let us also mention that, besides electromagnetic fields, there can be other effects that source a velocity to the axion field in the early universe and modify the conventional axion window. These include axion potentials with multiple hierarchically separated periods [18, 19], shift-symmetric couplings to gravity [20], derivative couplings to other coherent scalar fields such as the inflaton [21, 22], and an explicit breaking of the shift symmetry by higher-dimensional operators [23–25].

This paper is organized as follows: In Section 2 we give general discussions on the axion dynamics in a background of helical electromagnetic fields. In Section 3 we explicitly compute the effect of the helical fields on the relic abundance of axion-like particles and the QCD axion, and show how the parameter windows are affected. We conclude with a discussion of directions for further research in Section 4. In the appendix we analyze the cosmological evolution of helical electromagnetic fields.

2 Axion Dynamics with Helical Electromagnetic Fields

We consider an axion coupled to a U(1) gauge field,

$$\frac{\mathcal{L}}{\sqrt{-g}} = -\frac{1}{2}f^2 g^{\mu\nu} \partial_\mu \theta \partial_\nu \theta - m^2 f^2 (1 - \cos \theta) + \frac{\alpha}{8\pi} \theta F_{\mu\nu} \tilde{F}^{\mu\nu}. \quad (2.1)$$

Here the axion is written as a dimensionless angle θ , in terms of which the distance between the adjacent vacua is $\Delta\theta = 2\pi$. The mass m may or may not depend on the cosmic temperature, and f is the axion decay constant. The U(1) gauge field can be either the SM photon or a hidden photon, α is a dimensionless gauge coupling and can have either sign, and the dual field strength is

$$\tilde{F}^{\mu\nu} = \frac{1}{2} \eta^{\mu\nu\rho\sigma} F_{\rho\sigma}. \quad (2.2)$$

Here $\eta^{\mu\nu\rho\sigma} = \epsilon^{\mu\nu\rho\sigma} / \sqrt{-g}$ is a totally antisymmetric pseudotensor with the Levi-Civita symbol normalized as $|\epsilon^{0123}| = 1$.

Throughout this paper we consider cases where the global U(1) is already broken by the end of inflation, and continues to be broken in the post-inflationary epoch. Thus we impose

$$f > \frac{H_{\text{inf}}}{2\pi}, T_{\text{max}}, \quad (2.3)$$

where H_{inf} is the Hubble rate during inflation, T_{max} is the highest temperature achieved in the post-inflationary universe, and for simplicity we identified the symmetry breaking scale with the decay constant. The inflationary expansion sets the axion field to be spatially homogeneous throughout the observable universe, and gives rise to the vacuum misalignment scenario [26–28] for axion dark matter.

However, the basic picture of the vacuum misalignment becomes modified in the presence of a coherent $F\tilde{F}$ background, because the $\theta F\tilde{F}$ coupling sources an effective linear potential for the axion. This is also seen in the axion’s equation of motion. Fixing the metric to a flat FRW,

$$ds^2 = -dt^2 + a(t)^2 d\mathbf{x}^2, \quad (2.4)$$

the equation of motion for a homogeneous axion field reads

$$0 = \ddot{\theta} + 3H\dot{\theta} + m^2 \sin \theta - \frac{\alpha}{8\pi} \frac{F\tilde{F}}{f^2}. \quad (2.5)$$

Here, an overdot denotes a t -derivative, and $H = \dot{a}/a$. Before studying this equation in detail, we first discuss the physical meaning of $F\tilde{F}$.

2.1 Helical Electromagnetic Fields in the SM and Hidden Sector

The term $F\tilde{F}$ can be written as a dot product of electric and magnetic fields,

$$F_{\mu\nu}\tilde{F}^{\mu\nu} = -4E_\mu B^\mu, \quad (2.6)$$

where

$$E^\mu = u_\nu F^{\mu\nu}, \quad B^\mu = \frac{1}{2}\eta^{\mu\nu\rho\sigma} u_\sigma F_{\nu\rho}, \quad (2.7)$$

are the fields measured by a comoving observer with 4-velocity u^μ ($u_\mu u^\mu = -1$, $u^i = 0$; we use Latin letters to denote spatial indices). Even for a hidden U(1), we refer to the quantities in (2.7) as the ‘electric’ and ‘magnetic’ fields. As can be understood by noting that $F\tilde{F}$ is parity-odd, a nonvanishing $E \cdot B$ implies an asymmetry between the two circular polarization states, and hence such electromagnetic fields are referred to as ‘helical’ fields.

The energy density in the gauge field is a sum of the electromagnetic fields squared,¹ $\rho_A = (E_\mu E^\mu + B_\mu B^\mu)/2$. Then, noting that $(E_\mu \pm B_\mu)(E^\mu \pm B^\mu) \geq 0$, one finds that the magnitude of the product $E \cdot B$ is bounded by the energy density,

$$|E_\mu B^\mu| \leq \rho_A. \quad (2.8)$$

¹This can be checked by varying the gauge kinetic term $-FF/4$ with respect to the metric to obtain the energy-momentum tensor. Note that the interaction term $\theta F\tilde{F}$ does not contribute to the energy-momentum tensor.

Even if an electric field composed of the SM photons (or hypercharge gauge bosons) is produced in the early universe, it gets shorted out during the reheating epoch as the conductivity of the universe rises, after which $F\tilde{F}$ also vanishes. (For a discussion on the evolution of the conductivity, see e.g. [7].) However, SM electric fields may still survive until rather late times, if the reheating temperature is low, and also if the decay of the inflaton happens abruptly as in some models of preheating [29] instead of gradually through a perturbative decay. On the other hand, primordial electric fields composed of hidden photons that are decoupled from the SM remain intact during reheating, unless particles charged under the hidden U(1) are also produced. In the following we will mainly consider helical electromagnetic fields composed of hidden photons, however the analyses will also apply to the SM photon until the time when the electric field disappears.

If the U(1) gauge field is a hidden photon, then it behaves as extra radiation and contributes to the effective extra relativistic degrees of freedom of the universe via

$$\Delta N_A = \frac{8}{7} \left(\frac{11}{4} \right)^{4/3} \frac{\rho_A}{\rho_\gamma}, \quad (2.9)$$

with ρ_γ being the energy density in the SM photon. With this expression in mind, we can parameterize the amplitude of the dot product of the electric and magnetic fields as

$$\Delta N_{E \cdot B} \equiv \frac{8}{7} \left(\frac{11}{4} \right)^{4/3} \frac{|E_\mu B^\mu|}{\rho_\gamma} \leq \Delta N_A \lesssim 10^{-1}, \quad (2.10)$$

where the first inequality arises from (2.8) and is saturated for maximally helical fields. The second inequality shows the current constraint on extra radiation from CMB measurements [30]. After the electron-positron annihilation, the SM photon energy density redshifts as $\rho_\gamma \propto a^{-4}$. Hence if $E \cdot B$ also redshifts in a radiation-like manner of $E \cdot B \propto a^{-4}$, then $\Delta N_{E \cdot B}$ is time-independent.² However $E \cdot B$ can also exhibit other redshifting behaviors, depending on how the helical fields were originally produced.

In the following analyses we assume the helical electromagnetic fields to have been coherently produced in the early universe, and discuss their consequence for axions. A toy example of a gauge field theory that produces helical fields is discussed in Appendix A, where we also analyze the redshifting behaviors of the helical fields after being produced.

2.2 Induced Axion Velocity

Upon solving the equation of motion (2.5), let us for the moment ignore the axion potential, namely, we set $m = 0$. We further suppose that the background universe has a constant equation of state w , and that $F\tilde{F}$ is homogeneous and redshifts with some power of the scale factor,

$$H \propto a^{-\frac{3(w+1)}{2}}, \quad F\tilde{F} \propto a^{-n}. \quad (2.11)$$

Then the equation of motion (2.5) can be solved to yield the axion velocity as

$$\dot{\theta} = \left\{ -n + \frac{3(w+3)}{2} \right\}^{-1} \frac{\alpha}{8\pi} \frac{F\tilde{F}}{f^2 H} + K a^{-3}, \quad (2.12)$$

²If the dot product continues to redshift as $E_\mu B^\mu \propto a^{-4}$ until today, its present-day amplitude in Gauss (although these are electromagnetic fields in a hidden sector) is $|E_\mu B^\mu|_0 \sim (10^{-6} \text{ G})^2 \Delta N_{E \cdot B}$ in Heaviside-Lorentz units.

where we have assumed $n \neq 3(w+3)/2$, and K is an arbitrary constant. Without the source term, i.e. $F\tilde{F} = 0$, any initial velocity quickly decays away as $\dot{\theta} \propto a^{-3}$ as for any massless scalar in an expanding universe. However in the presence of an $F\tilde{F}$ background, the axion picks up a contribution $\dot{\theta} \propto \alpha F\tilde{F}/f^2 H$. This redshifts slower than a^{-3} and eventually dominates the axion velocity if $n < 3(w+3)/2$, which is satisfied, e.g., with $n = 4$ in a decelerating universe.³

The assumption of a negligible axion potential is justified if, in the equation of motion (2.5), the tilt of the $F\tilde{F}$ -induced linear potential is larger than that of the axion potential. This condition is written under $|\sin \theta| \sim 1$ as

$$\left| \frac{\alpha F\tilde{F}}{8\pi f^2} \right| > m^2. \quad (2.13)$$

The axion potential can be neglected also if the induced kinetic energy of the axion $\rho_{\theta \text{ kin}} = f^2 \dot{\theta}^2/2$ is larger than the height of the periodic axion potential $2m^2 f^2$, i.e.,

$$\left| \frac{\alpha F\tilde{F}}{8\pi f^2} \right| > mH, \quad (2.14)$$

where for simplicity we have assumed $|n - 3(w+3)/2| \sim 1$ and $K = 0$ in (2.12) for the axion velocity, and dropped order-unity factors. This condition implies that the axion is indeed able to go over the maxima of its periodic potential.

One may wonder what happens when only one of (2.13) or (2.14) is satisfied. In the case of $mH < |\alpha F\tilde{F}/8\pi f^2| < m^2$ (which necessarily entails $H < m$), the time it takes for the axion to move over the period of its potential $\Delta t = 2\pi/|\dot{\theta}|$ with velocity $|\dot{\theta}| \sim |\alpha F\tilde{F}/8\pi f^2 H|$, is shorter than the oscillation period $2\pi/m$ along the axion potential. This suggests that by averaging over a time interval shorter than $2\pi/m$, the axion potential in the equation of motion vanishes, i.e. $\langle m^2 \sin \theta \rangle \approx 0$, and thus it can be neglected. On the other hand if $m^2 < |\alpha F\tilde{F}/8\pi f^2| < mH$, the axion moves less than 2π in a Hubble time; in this case the axion moves with velocity $|\dot{\theta}| \sim |\alpha F\tilde{F}/8\pi f^2 H|$ but is trapped in a potential well over cosmological time scales.

Thus in summary, a coherent $F\tilde{F}$ background sources an axion velocity of

$$|\dot{\theta}| \sim \left| \frac{\alpha F\tilde{F}}{8\pi f^2 H} \right|, \quad (2.15)$$

given that its amplitude is as large as

$$\left| \frac{\alpha F\tilde{F}}{8\pi f^2} \right| > \min.\{m^2, mH\}. \quad (2.16)$$

³In the main part of the work [15], electric fields are considered to be zero and so is $F\tilde{F}$, and hence they make no mention of the specific solution $|\dot{\theta}| \sim |\alpha F\tilde{F}/8\pi f^2 H|$. The problem with their analysis is that they fix the integration constant by hand such that it depends on the magnetic helicity \mathcal{H}_B as $K \propto \alpha \mathcal{H}_B/f^2$. In this way they arrive at the incorrect conclusion that an axion velocity is induced by helical magnetic fields alone. They further argue that the relic abundance of the QCD axion depends linearly on the magnetic helicity, however we show in Section 3.2 that it actually depends on the amplitude of $E \cdot B$ with fractional powers.

2.3 Backreaction from the Axion

The axion can backreact to the gauge field, as a rolling axion itself induces excitation of the coupled gauge field. The effect becomes significant when the factor in front of $F\tilde{F}$ in the action (2.1) varies by a factor of order unity or larger within a Hubble time [10–13]. This condition can be written, using (2.15), as

$$\left| \frac{\alpha}{8\pi} \frac{\dot{\theta}}{H} \right| \sim \left(\frac{\alpha}{8\pi} \right)^2 \frac{|F\tilde{F}|}{f^2 H^2} > 1. \quad (2.17)$$

This is equivalent to saying that the induced kinetic energy of the axion is larger than $|F\tilde{F}|$. A coherent $F\tilde{F}$ as large as (2.17) moves the axion rapidly in one direction, which in turn is expected to produce gauge bosons with momenta typically of order the Hubble scale at that time. This process should slow down the axion velocity, and also implies the cascading of the power of $F\tilde{F}$ towards higher momenta. A detailed study of the axion electrodynamics in such a regime will likely require lattice studies and is beyond the scope of this work, however it would be very interesting to investigate the possibility of the axion-induced UV cascade of helical electromagnetic fields.⁴

2.4 Onset of Axion Oscillation

In the conventional vacuum misalignment scenario without an $F\tilde{F}$ background, the axion field stays frozen at some initial value while $H > m$, then begins to oscillate about a potential minimum when $H \sim m$. Henceforth we use the subscript “ m ” to denote quantities at the time the Hubble rate becomes equal to the axion mass (note that the mass may also vary in time),

$$H_m = m_m. \quad (2.18)$$

The energy density of the axion at the onset of the oscillation is

$$\rho_{\theta m} = b (m^2 f^2 \theta^2)_m, \quad (2.19)$$

where the cosine potential has been expanded around zero assuming $|\theta_m| \lesssim 1$, and b is a factor of order unity. From then on, the axion oscillates and its particle number is conserved, so the physical number density $n_\theta = \rho_\theta/m$ redshifts as a^{-3} . The relic abundance today is thus obtained as

$$\rho_{\theta 0} = m_0 n_{\theta 0} = b m_0 m_m f^2 \theta_m^2 \left(\frac{a_m}{a_0} \right)^3, \quad (2.20)$$

where the subscript “0” is used to denote quantities in the present universe.

Now, in the presence of an $F\tilde{F}$ background, given that both H/m and $|F\tilde{F}/mH|$ monotonically decrease in time, there are two possible scenarios. The first is the case where the condition (2.16) is never satisfied after the time of $H = m$. It may have been satisfied while $H > m$, however this merely moves the axion field prior to the onset of the oscillation. Hence the effect of $F\tilde{F}$ can be absorbed by a shift in the value of θ_m , and the axion’s relic abundance is given by (2.20).

⁴If $|(\alpha/8\pi)(\dot{\theta}/H)|$ is sufficiently larger than unity during inflation, it can also generate large non-Gaussianities in the curvature perturbation and/or violate perturbativity, see e.g. [31, 32]. We also note that, while here we discussed the backreaction from the rolling axion, gauge field excitations may also happen during the oscillatory phase [33, 34].

The story is drastically modified if the condition (2.16) continues to hold after the time of $H = m$, namely, if

$$\left| \frac{\alpha (F\tilde{F})_m}{8\pi f^2} \right| > m_m^2. \quad (2.21)$$

In this case the axion continues to move in one direction with the velocity (2.15) even at times when $H < m$, until the condition (2.16) is saturated when $|\alpha F\tilde{F}/8\pi f^2|$ becomes equal to mH ; we denote quantities then by the subscript “tr”, namely,

$$\left| \frac{\alpha (F\tilde{F})_{\text{tr}}}{8\pi f^2} \right| = (mH)_{\text{tr}}. \quad (2.22)$$

At this time the axion’s kinetic and potential energies become comparable, and hence the axion gets trapped in its potential well and begins to oscillate about a minimum. Supposing that upon trapping the axion field is displaced from the nearest potential minimum by $|\theta_{\text{tr}} - \theta_{\text{min}}| \sim 1$, the axion’s energy density is written as

$$\rho_{\theta \text{tr}} = c m_{\text{tr}}^2 f^2, \quad (2.23)$$

with c being a factor of order unity. Hereafter we can follow the same steps as for the conventional misalignment scenario, and obtain the relic abundance as

$$\rho_{\theta 0} = c m_0 m_{\text{tr}} f^2 \left(\frac{a_{\text{tr}}}{a_0} \right)^3. \quad (2.24)$$

Comparing this result with (2.20), one sees that the net effect of an $F\tilde{F}$ background satisfying (2.21) is to enhance the axion relic abundance by delaying the onset of the oscillation from when $H \sim m$ to the time of trapping described by (2.22).

We should remark that the approximation (2.24) with $c \sim 1$ can break down if the coefficient $|n - 3(w + 3)/2|^{-1}$ in (2.12) that we have dropped is much larger (smaller) than unity; in such cases the time of the trapping will deviate from (2.22), leading to an enhancement (suppression) of the final abundance. In addition, if $|\theta_{\text{tr}} - \theta_{\text{min}}| \approx \pi$, then the relic abundance will be enhanced by anharmonic effects [35, 36] (the same is true for the expression (2.20) for the conventional scenario).

2.5 Numerical Example

We verified the axion dynamics discussed above by numerically solving the equation of motion (2.5), whose results are shown in Figure 1. Here we have set the background Hubble parameter and helical fields to redshift following the form of (2.11), with powers $w = 1/3$ and $n = 4$. We took the axion mass to be a constant, and started the computation from the time when $H = 10^3 m$, with an initial condition $\theta_{\text{ini}} = 1$ and velocity (2.12) with $K = 0$. The time evolution of the axion field is shown in the left panel as a function of a/a_m , in log-linear scale. Here we have limited the displayed range to $-\pi \leq \theta \leq \pi$ by identifying the points $\theta = \pm\pi$, so that the minimum around which the axion eventually oscillates is $\theta = 0$. Shown are three cases in which the $F\tilde{F}$ amplitude, parameterized as

$$R_m = \left| \frac{\alpha (F\tilde{F})_m}{8\pi m^2 f^2} \right|, \quad (2.25)$$

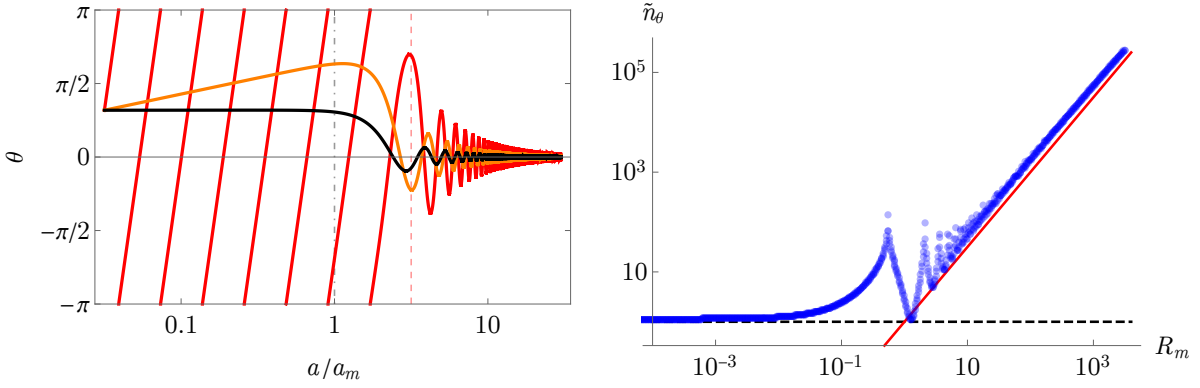


Figure 1: Left: Time evolution of the axion angle as a function of the scale factor, in log-linear scale. The upper and lower edges are identified. The amplitude of $F\tilde{F}$ is varied, in terms of the normalized quantity (2.25), as $R_m \ll 0.1$ (black curve), $R_m = 0.3$ (orange), and $R_m = 10$ (red). The dot-dashed vertical line shows when $a = a_m$, and the red dashed vertical line is $a = a_{tr}$ for $R_m = 10$. When $F\tilde{F}$ is sufficiently large, the axion is forced to move through multiple periods, and the onset of the axion oscillation is delayed. Right: Normalized comoving number density of the axion in the asymptotic future, as a function of R_m . The blue dots show the numerical results, while the black dashed and red solid lines show analytic estimates. See the text for details.

is chosen as $R_m \ll 0.1$ (black curve), $R_m = 0.3$ (orange), and $R_m = 10$ (red). This parameterization is introduced such that the condition (2.21) corresponds to $R_m > 1$. The results displayed in this subsection are independent of the exact values of $\alpha F\tilde{F}$, m , f , etc. However we note that we have chosen the sign as $\alpha F\tilde{F} > 0$, which forces the axion to move towards the positive direction. For $R_m \ll 0.1$, it is seen that the effect of $F\tilde{F}$ is negligible and the axion dynamics is the same as in the conventional misalignment scenario, in which the axion begins to oscillate at around $a = a_m$, indicated by the dot-dashed vertical line. For $R_m = 0.3$, the axion also begins oscillating at $a \sim a_m$, however until the oscillation the $F\tilde{F}$ background forces the axion to move away from its initial position. The case of $R_m = 10$ satisfies (2.21), and the axion moves through multiple periods until the time $a = a_{tr}$, which is indicated by the red dashed vertical line. Further increasing R_m yields an even larger separation between a_m and a_{tr} .

We also carried out the computations for a wide range of values for R_m ; in the right panel we plot the comoving axion number density ($\propto n_\theta a^3$) evaluated after the axion has begun its oscillation and the number become conserved, as a function of R_m (the sign is chosen as $\alpha F\tilde{F} > 0$). The numerical results are shown as the blue dots, and the comoving number density in the y -axis is normalized as

$$\tilde{n}_\theta = \frac{n_\theta}{m f^2} \left(\frac{a}{a_m} \right)^3. \quad (2.26)$$

One can also analytically calculate this quantity using (2.20) and (2.24) with $w = 1/3$, $n = 4$, and by setting $\theta_m = b = c = 1$, as

$$\tilde{n}_\theta = \begin{cases} 1 & \text{for } R_m < 1, \\ R_m^{\frac{6}{2n-3(w+1)}} = R_m^{3/2} & \text{for } R_m \geq 1. \end{cases} \quad (2.27)$$

$$(2.28)$$

These are shown in the plot as the black dashed and red solid lines, respectively. One sees that the

analytic expressions with $b = 1$ and $c = 1$ are consistent at the order-of-magnitude level with the numerical results in the asymptotic regions $R_m \ll 1$ and $R_m \gg 1$.

The oscillatory behavior of \tilde{n}_θ , which is most prominent around $R_m \sim 1$, is due to the $F\tilde{F}$ background shifting the misalignment angle with a periodicity of 2π ; such an effect is not captured in the analytic estimate where we have fixed the misalignment to unity for simplicity. The oscillation peaks of \tilde{n}_θ correspond to the axion being placed near the hilltop $\theta = \pm\pi$ at the onset of the oscillation, which gives anharmonic enhancements to the relic abundance. We remark that, since we have carried out the computations only for a finite number of values of R_m , the plot does not fully uncover the shape of the anharmonic peaks. Note also that in the extremely anharmonic region, axionic domain walls are expected to form, and thus one will have to include spatial inhomogeneities into the analyses. We should also mention that, as one increases R_m much beyond unity, the backreaction from the axion will become non-negligible at $R_m > 8\pi/|\alpha|$, as can be seen from the criteria (2.17).

3 Axion Relic Abundance

3.1 Constant-Mass Axion

As the simplest example, we begin by considering an axion whose mass m is a constant parameter. We assume this axion to be coupled to hidden photons that make up helical electromagnetic fields. Moreover, to make our discussion concrete, we assume the helical fields to redshift in a radiation-like manner, i.e.,

$$F\tilde{F} \propto a^{-4}. \quad (3.1)$$

We also suppose the universe at the time of $H = m$ to be dominated by radiation, and the entropy of the universe to be conserved thereafter, so that the entropy density redshifts as $s \propto a^{-3}$. These assumptions allow us to write $(F\tilde{F})_m = (F\tilde{F})_0 (s_m/s_0)^{4/3}$. Further noting that the Hubble rate and the entropy density during radiation domination are expressed in terms of the cosmic temperature as

$$3M_{\text{Pl}}^2 H^2 \simeq \rho_{\text{rad}} = \frac{\pi^2}{30} g_*(T) T^4, \quad s = \frac{2\pi^2}{45} g_{*s}(T) T^3, \quad (3.2)$$

the entropy density at $H = m$ can be written as

$$s_m = \left(\frac{128\pi^2}{45} \right)^{1/4} \frac{g_{*s}(T_m)}{g_*(T_m)^{3/4}} (m M_{\text{Pl}})^{3/2}. \quad (3.3)$$

Thus the condition (2.21) for the helical fields to delay the onset of the axion oscillation is translated into a lower bound on the field values today,

$$\left| \frac{\alpha}{8\pi} (F\tilde{F})_0 \right| > \left(\frac{45}{128\pi^2} \right)^{1/3} \frac{g_*(T_m)}{g_{*s}(T_m)^{4/3}} \frac{f^2 s_0^{4/3}}{M_{\text{Pl}}^2}. \quad (3.4)$$

Under this condition $a_{\text{tr}} > a_m$, and hence one can also solve for s_{tr} by combining (2.22), that is,

$$m H_{\text{tr}} = \left| \frac{\alpha}{8\pi} \frac{(F\tilde{F})_{\text{tr}}}{f^2} \right| = \left| \frac{\alpha}{8\pi} \frac{(F\tilde{F})_0}{f^2} \right| \left(\frac{s_{\text{tr}}}{s_0} \right)^{4/3}, \quad (3.5)$$

with (3.2) which can be used to rewrite H_{tr} in terms of s_{tr} . Then substituting $(a_{\text{tr}}/a_0)^3 = s_0/s_{\text{tr}}$ into (2.24) gives

$$\rho_{\theta 0} = c \left(\frac{128\pi^2}{45} \right)^{1/4} \frac{g_{*s}(T_{\text{tr}})}{g_*(T_{\text{tr}})^{3/4}} \left| \frac{\alpha}{8\pi} (F\tilde{F})_0 \right|^{3/2} \frac{m^{1/2} M_{\text{Pl}}^{3/2}}{f s_0}, \quad (3.6)$$

where the power 3/2 of the $|\alpha F\tilde{F}|$ term corresponds to that of R_m in the expression (2.28). We can further rewrite $|F\tilde{F}|_0$ in terms of $\Delta N_{E\cdot B}$ defined in (2.10), by noting that $\Delta N_{E\cdot B}$ becomes constant after the electron-positron annihilation due to the assumption of $F\tilde{F} \propto a^{-4}$. Then, plugging in numbers for the physical constants and cosmological parameters, and also setting $c \sim 1$ and $g_{*s}/g_*^{3/4} \sim 1$, the axion abundance (3.6) and the condition (3.4) are written as

$$\Omega_{\theta} h^2 \sim 10^{-1} \left(\frac{|\alpha| \Delta N_{E\cdot B}}{10^{-2}} \right)^{3/2} \left(\frac{f}{10^{17} \text{ GeV}} \right)^{-1} \left(\frac{m}{10^{-22} \text{ eV}} \right)^{1/2} \quad (3.7)$$

for $|\alpha| \Delta N_{E\cdot B} \gtrsim 10^{-2} \left(\frac{f}{10^{17} \text{ GeV}} \right)^2$.

Here the abundance is expressed in units of the present value of the critical density, and h is the dimensionless Hubble parameter. Here and below $\Delta N_{E\cdot B}$ is the value after the electron-positron annihilation, and note that the axion abundance depends on the helical fields through the combination $|\alpha| \Delta N_{E\cdot B}$.

On the other hand, if the amplitude of the helical fields is small enough such that (2.21) is not satisfied, then the conventional vacuum misalignment scenario is recovered. The abundance is computed as (2.20), giving the familiar result [37],

$$\Omega_{\theta} h^2 \sim 10^{-1} \theta_m^2 \left(\frac{f}{10^{17} \text{ GeV}} \right)^2 \left(\frac{m}{10^{-22} \text{ eV}} \right)^{1/2} \quad \text{for } |\alpha| \Delta N_{E\cdot B} \lesssim 10^{-2} \left(\frac{f}{10^{17} \text{ GeV}} \right)^2. \quad (3.8)$$

Note that if $|\alpha| \Delta N_{E\cdot B}$ is non-zero, the misalignment angle θ_m when the axion begins to oscillate can be different from the value at earlier times, say, at the end of inflation.

One can collectively write the axion abundance in the two regimes (3.7) and (3.8) as:

$$\Omega_{\theta} h^2 \sim 10^{-1} \left(\frac{m}{10^{-22} \text{ eV}} \right)^{1/2} \left(\frac{f}{10^{17} \text{ GeV}} \right)^{-1} \left[\max. \left\{ \left(\frac{|\alpha| \Delta N_{E\cdot B}}{10^{-2}} \right), \left(\frac{f}{10^{17} \text{ GeV}} \right)^2 \right\} \right]^{3/2}, \quad (3.9)$$

where we have ignored the possibility of a fine-tuned initial angle and thus set $\theta_m^2 \sim 1$ in (3.8). This expression clearly shows that helical electromagnetic fields, when large enough, have the effect of increasing the axion abundance.

Let us also assess the backreaction from the axion to the gauge field. With $F\tilde{F} \propto a^{-4}$, the ratio $F\tilde{F}/H^2$ stays more or less constant during radiation domination, hence we evaluate the backreaction condition (2.17) at the time of the trapping (2.22). (Note that this condition can be satisfied only by helical fields large enough to delay the axion oscillation, i.e. (2.21), unless $|\alpha|$ exceeds 8π .) Supposing $F\tilde{F} \propto s^{4/3}$ to hold after the trapping, and rewriting s in terms of H using (3.2), we obtain

$$\left| \frac{F\tilde{F}}{f^2 H^2} \right|_{\text{tr}} = \left(\frac{128\pi^2}{45} \right)^{1/3} \frac{g_{*s}(T_{\text{tr}})^{4/3}}{g_*(T_{\text{tr}})} \frac{|F\tilde{F}|_0 M_{\text{Pl}}^2}{f^2 s_0^{4/3}}. \quad (3.10)$$

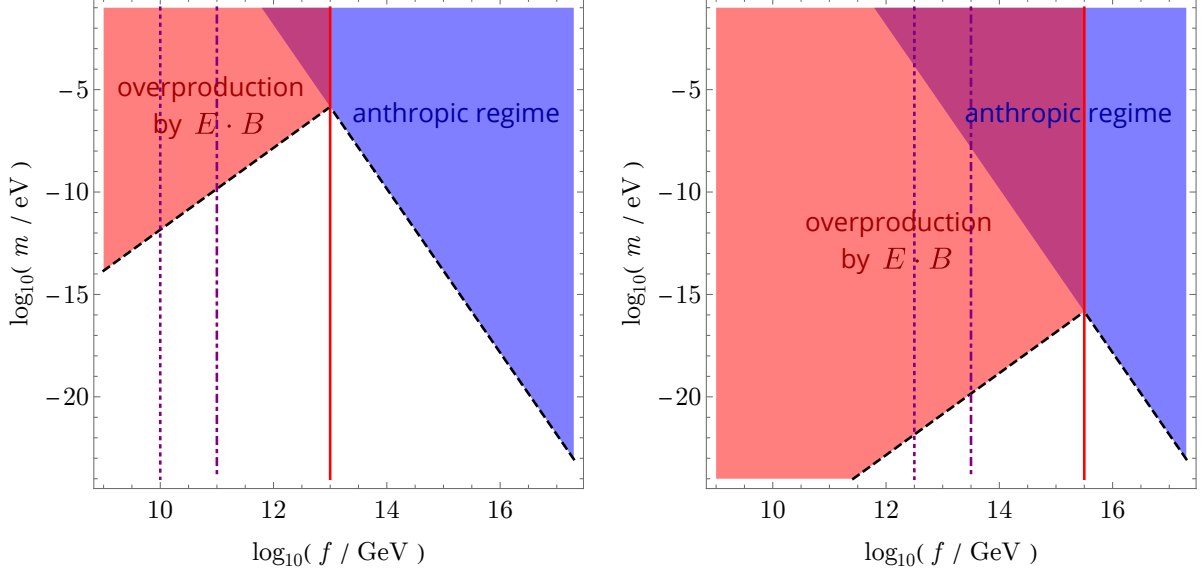


Figure 2: Window of constant-mass axions in the presence of helical electromagnetic fields. Axes are the axion decay constant and mass, and the amplitude of the helical fields are taken as $|\alpha|\Delta N_{E\cdot B} = 10^{-10}$ (left panel), 10^{-5} (right). The axion makes up the entire dark matter density on the black dashed line. The helical fields enhance the axion abundance on the left side of the red solid line, and overproduces axion dark matter in the red region. The blue region shows where axion dark matter is overproduced in the conventional vacuum misalignment scenario, unless the misalignment angle is tuned. Backreactions from the axion to the helical fields are non-negligible on the left side of the purple dotted (dot-dashed) lines for $|\alpha| = 10^{-4}$ (10^{-2}).

Using this and setting $g_{*s}^{4/3}/g_* \sim 1$, one finds that the backreaction is non-negligible if

$$\alpha^2 \Delta N_{E\cdot B} \gtrsim \left(\frac{f}{10^{17} \text{ GeV}} \right)^2. \quad (3.11)$$

Note that the strength of backreaction depends on $\alpha^2 \Delta N_{E\cdot B}$, while the axion abundance is set by $\alpha \Delta N_{E\cdot B}$.

In Figure 2, we show the axion window in terms of f and m . The left panel is the case with $|\alpha|\Delta N_{E\cdot B} = 10^{-10}$, and the right is $|\alpha|\Delta N_{E\cdot B} = 10^{-5}$. The lower edge of the blue region shows the parameter combinations in the conventional misalignment scenario (cf. (3.8)) for which an axion makes up the entire dark matter abundance, i.e. $\Omega_\theta h^2 \approx 0.1$, with an initial angle $|\theta_m| \approx 1$. Inside the blue region, the axion gives too much dark matter in the universe, unless the initial angle takes fine-tuned values of $|\theta_m| \ll 1$ (the ‘‘anthropic window’’). The condition of (2.21) is satisfied in the left side of the red solid line, where the onset of the axion oscillation is delayed by the helical electromagnetic fields and thus the relic abundance is given by (3.7). Here, $\Omega_\theta h^2 \approx 0.1$ is realized on the lower edge of the red region, while inside the red region axion dark matter is overproduced. The parameter window affected by the helical fields expands to larger f with increasing $|\alpha|\Delta N_{E\cdot B}$. Putting together the regions affected/unaffected by the helical fields, the black dashed line shows where $\Omega_\theta h^2 \approx 0.1$ without a fine-tuned initial condition. However we should remark that the backreaction from the axion to the helical fields becomes non-negligible, i.e. (3.11), on the left

side of the purple dotted line for $|\alpha| = 10^{-4}$, and the purple dot-dashed line for $|\alpha| = 10^{-2}$. (For these values of $|\alpha|$, the choices of $|\alpha|\Delta N_{E.B}$ in the plots imply $\Delta N_{E.B} \leq 10^{-1}$, being compatible with the observational constraint (2.10) on extra radiation. The rate of decay of the axion into hidden photons via $(\alpha/8\pi)\theta F\tilde{F}$ is also small such that the axion lifetime is longer than the age of the universe in the entire parameter range shown in the plots.) As the gauge coupling $|\alpha|$ becomes larger, the strong-backreaction region spreads towards larger f . Here the axion is expected to induce a UV cascading of the helical fields and thus the calculation (3.7) of the abundance may become invalid.⁵ We also note that in the plots we have used the order-of-magnitude estimates (3.7) and (3.8), which ignore the possibility of the initial misalignment angle and $|\alpha|F\tilde{F}$ conspiring to give anharmonic enhancements of the axion abundance, as depicted by the oscillation peaks in the right panel of Figure 1. This effect can further transform the axion window.

Let us also comment on the implication for ultralight axion dark matter [37, 38] with $m \lesssim 10^{-21}$ eV, which is constrained by studies of the Lyman- α forest [39–41] and galaxy rotation curves [42]. For axions in this mass regime to make up most of the dark matter, the conventional misalignment scenario requires $f \gtrsim 10^{17}$ GeV. However with an $F\tilde{F}$ background, axions with much smaller decay constants can also account for ultralight dark matter and leave distinct signatures in the small-scale structures of the universe.

3.2 QCD Axion

We now study the impact of an $F\tilde{F}$ background on the QCD axion [1–3], whose mass depends on the cosmic temperature approximately as

$$m(T) \simeq \begin{cases} \lambda m_0 \left(\frac{\Lambda_{\text{QCD}}}{T}\right)^p & \text{for } T \gg \Lambda_{\text{QCD}}, \\ m_0 & \text{for } T \ll \Lambda_{\text{QCD}}. \end{cases} \quad (3.12)$$

Here $\Lambda_{\text{QCD}} \approx 200$ MeV, $\lambda \approx 0.1$, $p \approx 4$, and the zero-temperature mass is given by [43, 44]

$$m_0 \approx 6 \times 10^{-6} \text{ eV} \left(\frac{10^{12} \text{ GeV}}{f}\right). \quad (3.13)$$

Let us again suppose the helical fields to be composed of hidden photons with a redshifting behavior $F\tilde{F} \propto a^{-4}$, and that the universe becomes radiation-dominated by the time when $H = m$. The calculations can be carried out similarly to the previous section, except for that now the axion mass also varies in time. We focus on axions with decay constants of $f \lesssim 10^{17}$ GeV, for which the Hubble rate becomes equal to the axion mass at temperatures $T_m \gtrsim \Lambda_{\text{QCD}}$, giving $m(T_m) \simeq \lambda m_0 (\Lambda_{\text{QCD}}/T_m)^p$.

We begin by considering $F\tilde{F}$ whose amplitude is so large that the onset of the axion oscillation is delayed to times when the cosmic temperature has dropped below the QCD scale, i.e. $T_{\text{tr}} \lesssim \Lambda_{\text{QCD}} \lesssim T_m$. For this case the mass is already a constant when the oscillation begins, i.e., $m(T_{\text{tr}}) \simeq m_0$, so the relic abundance for constant-mass axions (3.7) applies by simply replacing $m \rightarrow m_0$. However the lower bound on $F\tilde{F}$ is now stronger, as we are imposing $T_{\text{tr}} \lesssim \Lambda_{\text{QCD}}$. We slightly modify this

⁵The calculation may also break down when $\Delta N_{E.B}$ is so large that the hidden photon and/or the axion dominate over the SM radiation already in the early universe, hence violating our assumption of radiation domination at $H = m$.

condition to $\lambda(\Lambda_{\text{QCD}}/T_{\text{tr}})^p > 1$ so that $m(T_{\text{tr}}) \simeq m_0$ under the expression (3.12); then by solving for T_{tr} as discussed around (3.5), one finds the bound

$$\left| \frac{\alpha}{8\pi} (F\tilde{F})_0 \right| > \frac{1}{2} \left(\frac{45}{2\pi^2} \right)^{5/6} \frac{g_*(T_{\text{tr}})^{1/2}}{g_{*s}(T_{\text{tr}})^{4/3}} \frac{m_0 f^2 s_0^{4/3}}{\lambda^{2/p} \Lambda_{\text{QCD}}^2 M_{\text{Pl}}}. \quad (3.14)$$

Also noting that the zero-temperature mass of the QCD axion is a function of the decay constant, cf. (3.13), and plugging in numbers, the abundance is obtained as

$$\Omega_\theta h^2 \sim 10^{-1} \left(\frac{|\alpha| \Delta N_{E.B}}{10^{-11}} \right)^{3/2} \left(\frac{f}{10^{12} \text{ GeV}} \right)^{-3/2} \quad \text{for } |\alpha| \Delta N_{E.B} \gtrsim 10^{-6} \left(\frac{f}{10^{12} \text{ GeV}} \right). \quad (3.15)$$

Even if $F\tilde{F}$ is not as large as shown in (3.15), it still impacts the QCD axion abundance as long as it is large enough to delay the onset of the oscillation to times when $H < m$, namely, if $\Lambda_{\text{QCD}} \lesssim T_{\text{tr}} < T_m$. In this case the mass continues to vary in time after the axion trapping. The lower bound for $F\tilde{F}$ arises from (2.21), which turns out to take exactly the same form as (3.4). One can solve for T_{tr} using $m(T_{\text{tr}}) \simeq \lambda m_0 (\Lambda_{\text{QCD}}/T_{\text{tr}})^p$, and derive the relic abundance as

$$\rho_{\theta 0} = c \left\{ \frac{2\pi^2}{45} \frac{g_{*s}(T_{\text{tr}})}{\lambda \Lambda_{\text{QCD}}^p m_0^2 f^2 s_0} \right\}^{\frac{1}{p+2}} \left\{ 2 \left(\frac{45}{2\pi^2} \right)^{1/6} \frac{g_{*s}(T_{\text{tr}})^{1/3}}{g_*(T_{\text{tr}})^{1/2}} \left| \frac{\alpha}{8\pi} (F\tilde{F})_0 \right| \frac{m_0 M_{\text{Pl}}}{s_0^{1/3}} \right\}^{\frac{p+3}{p+2}}. \quad (3.16)$$

Thus we find

$$\Omega_\theta h^2 \sim 10^{-1} \left(\frac{|\alpha| \Delta N_{E.B}}{10^{-12}} \right)^{7/6} \left(\frac{f}{10^{12} \text{ GeV}} \right)^{-7/6} \quad (3.17)$$

$$\text{for } 10^{-12} \left(\frac{f}{10^{12} \text{ GeV}} \right)^2 \lesssim |\alpha| \Delta N_{E.B} \lesssim 10^{-6} \left(\frac{f}{10^{12} \text{ GeV}} \right).$$

The lower bound on $|\alpha| \Delta N_{E.B}$ is equivalent to that in (3.7), however the reference value for f has been changed.

An even smaller $F\tilde{F}$ merely shifts the axion field value prior to the onset of the oscillation at $H \sim m$, and the abundance takes the familiar expression (2.20) from the conventional misalignment scenario [35]:

$$\Omega_\theta h^2 \sim 10^{-1} \theta_m^2 \left(\frac{f}{10^{12} \text{ GeV}} \right)^{7/6} \quad \text{for } |\alpha| \Delta N_{E.B} \lesssim 10^{-12} \left(\frac{f}{10^{12} \text{ GeV}} \right)^2. \quad (3.18)$$

In summary, the relic abundance of the QCD axion takes the forms (3.15), (3.17), and (3.18), depending on the amplitude of the $F\tilde{F}$ background. One immediately finds that the expression (3.15) in the large $|\alpha| \Delta N_{E.B}$ regime gives $\Omega_\theta h^2 \gtrsim 10^6$, indicating an overproduction of axion dark matter. (Note that this simply implies that the axion density would be much larger than the measured value of the critical density, but it does not mean that the axion would actually “overclose” the universe.) We also note that the condition for significant backreaction (3.11) applies for the QCD axion in exactly the same form, as its derivation is independent of the time evolution of the mass.

In Figure 3, we show the axion window in terms of f and $|\alpha| \Delta N_{E.B}$. On the left edge of the blue region, i.e. $f \sim 10^{12} \text{ GeV}$, the axion makes up the entire dark matter abundance in the conventional

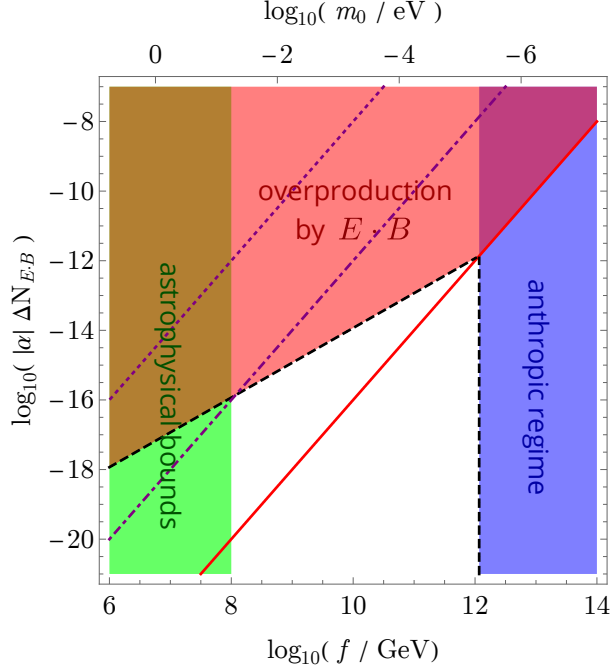


Figure 3: QCD axion window in the presence of helical electromagnetic fields. Axes are the axion decay constant (bottom), zero-temperature mass (top), and the amplitude of the helical fields (left). The axion makes up the entire dark matter density on the black dashed line. The helical fields enhance the axion abundance on the left side of the red solid line, and overproduce axion dark matter in the red region. The blue region shows where axion dark matter is overproduced in the conventional vacuum misalignment scenario, unless the misalignment angle is tuned. The green region is excluded from astrophysical observations. Backreactions from the axion to the helical fields are non-negligible on the left side of the purple dotted (dot-dashed) lines for $|\alpha| = 10^{-6}$ (10^{-2}).

misalignment scenario (cf. (3.18)), with an initial angle $|\theta_m| \approx 1$. Inside the blue region, axion dark matter is overproduced unless the initial angle is tuned to $|\theta_m| \ll 1$. The condition (2.21) is satisfied in the left side of the red solid line, where the relic abundance directly depends on the helical field amplitude as (3.15) or (3.17). $\Omega_\theta h^2 \approx 0.1$ is realized on the lower edge of the red region, where the abundance is given by (3.17), and inside the red region axion dark matter is overproduced. Putting together the regions affected/unaffected by the helical fields, the black dashed line shows where $\Omega_\theta h^2 \approx 0.1$ without a fine-tuned initial condition. The backreaction from the axion to the helical fields become non-negligible, i.e. (3.11), on the left side of the purple dotted line for $|\alpha| = 10^{-6}$, and the purple dot-dashed line for $|\alpha| = 10^{-2}$. (These values of $|\alpha|$ give $\Delta N_{E \cdot B} \leq 10^{-1}$ and a negligibly small decay rate of the axion into hidden photons in the entire displayed area.) In these backreaction regions the results (3.15) and (3.17) may become invalid. The green region is excluded by astrophysical studies setting lower bounds of $f \gtrsim 10^8$ GeV on the QCD axion decay constant [45]. For axions marginally satisfying this astrophysical bound, one sees from the plot that the oscillation is delayed by helical fields as small as $|\alpha| \Delta N_{E \cdot B} \sim 10^{-20}$. Moreover, for $|\alpha| \Delta N_{E \cdot B} \gtrsim 10^{-12}$, the

conventional QCD axion window $10^8 \text{ GeV} \lesssim f \lesssim 10^{12} \text{ GeV}$ is completely closed.⁶ In the conventional misalignment scenario, for axions with $f < 10^{12} \text{ GeV}$ to make up the entire dark matter abundance, one would need to invoke a tuned initial condition of $|\theta|_m \approx \pi$ so that the abundance receives anharmonic enhancements, although this would also enhance isocurvature perturbations and thus is constrained by CMB measurements [46]. We find that helical electromagnetic fields can allow such low- f axions to be abundantly produced without invoking anharmonic effects.

4 Conclusions and Discussion

Our main message is that primordial electromagnetic fields can strongly impact the cosmic evolution of axions, and vice versa. In this paper, we have shown that helical electromagnetic fields coherently excited in the early universe induce a field velocity to the coupled axion. If the amplitude of $E \cdot B$ is large enough such that the induced kinetic energy of the axion is larger than the height of the axion potential at the time when $H \sim m$, then the axion continues to roll in one direction and the onset of the axion oscillation is delayed, leading to an enhancement of the final axion abundance. For a QCD axion coupled to a hidden U(1) gauge field, the abundance was derived as (3.15), (3.17), and (3.18), depending on the helical field amplitude. In particular, we found that the conventional window $10^8 \text{ GeV} \lesssim f \lesssim 10^{12} \text{ GeV}$ becomes completely closed due to overproduction of axion dark matter, with helical fields as small as $|\alpha|\Delta N_{E \cdot B} \gtrsim 10^{-12}$, where α is the gauge coupling and $\Delta N_{E \cdot B}$ parametrizes the amplitude of $E \cdot B$ in terms of the effective extra relativistic degrees of freedom. Comparing with the current observational constraint on extra radiation $\Delta N_{E \cdot B} \lesssim 10^{-1}$, there is a wide range of parameters for which hidden helical fields trigger an overproduction of the QCD axion. For an axion-like particle with a constant mass, its abundance is given by (3.7) and (3.8). The window of axion-like particles was also found to be significantly modified by rather weak helical fields. One implication of the results is that, for axions in the ultralight mass range $m \lesssim 10^{-21} \text{ eV}$ to make up the entire dark matter and leave distinct signatures in the small-scale structures of the universe, the required value of the decay constant in the presence of an $E \cdot B$ becomes $f \ll 10^{17} \text{ GeV}$, being much smaller than in the conventional misalignment scenario. Our results can further be used to put constraints on early universe models that give rise to helical electromagnetic fields, from the requirement that axion dark matter not be overproduced.

In order to explicitly compute the axion abundance, we focused on a case where the axion couples to a hidden U(1) field; this field was considered to make up helical electromagnetic fields that are homogeneous over the entire observable universe, and whose dot product redshifts as $E \cdot B \propto a^{-4}$. We also supposed the spontaneous breaking of the global U(1) symmetry to happen before inflation. Let us comment on each of these assumptions and discuss directions for further study.

- *SM/hidden, Abelian/non-Abelian gauge field.* We mainly considered a hidden U(1) gauge field that is decoupled from the SM, such that the hidden electric field survives the reheating epoch. However we remark that the SM electromagnetic field can also enhance the axion abundance, if the reheating temperature is sufficiently low and the conductivity of the universe stays

⁶This can also be derived from (3.17) and (3.18) which indicate that, for $\theta_m^2 \sim 1$ and a fixed $|\alpha|\Delta N_{E \cdot B}$, the axion abundance is minimized at $f \sim 10^{18} \text{ GeV} (|\alpha|\Delta N_{E \cdot B})^{1/2}$ as $(\Omega_\theta h^2)_{\min} \sim 10^6 (|\alpha|\Delta N_{E \cdot B})^{7/12}$.

tiny⁷ until the time when $H \sim m$. It would also be interesting to apply our discussions to non-Abelian gauge fields and study effects from, for instance, color electromagnetic fields.

- *Homogeneous/inhomogeneous electromagnetic fields.* The actual spectrum of primordial electromagnetic fields depends on the excitation mechanism of the gauge fields. We have considered the Fourier modes of the electromagnetic fields to be concentrated at wavelengths larger than the present Hubble radius, and studied uniform effects on the axion in the entire visible universe. If instead the fields have small-wavelength components, then the axion is forced to move differently in each patch of the universe. This gives rise to isocurvature perturbations of the axion density, and even the formation of axionic domain walls if the helical field amplitude is sufficiently large. Inhomogeneous electromagnetic fields also imply that the (dark) radiation density itself fluctuates, which may be constrained from observations.
- *Redshifting of helical electromagnetic fields.* We discussed in Appendix A that $E \cdot B$ may exhibit a redshifting behavior other than the radiation-like $\propto a^{-4}$, depending on how it is originally produced. In such cases, the dependence of the axion abundance on $\Delta N_{E \cdot B}$ would be modified from our results.
- *Spontaneous symmetry breaking before/after inflation.* We focused on cases where the global U(1) breaks before inflation, and studied how the vacuum misalignment scenario is affected by the presence of helical electromagnetic fields. Here we note that the conventional misalignment scenario assumes that during inflation the Hubble rate is larger than the axion mass; otherwise the axion would be stabilized at the potential minimum and thus the axion particles cannot be produced. However, even with a low-scale inflation whose Hubble rate is smaller than the axion mass, helical electromagnetic fields can kick the axion out of the vacuum and produce axion dark matter. (See also [21,22] for a closely related idea.) On the other hand, a symmetry breaking after inflation gives rise to cosmic strings and domain walls. Helical fields should also have an effect on this scenario, especially on the formation of the walls due to the periodic axion potential.
- *Generation of helical electromagnetic fields.* The primary goal of the present work is to illustrate the impact of helical electromagnetic fields on the axion evolution, and hence we did not specify how the helical fields have been generated. Clearly an important direction for further work is investigating the generation mechanisms, which is also required for understanding the redshifting behavior of the helical fields in the later universe. For a recent study of a generation model for large-scale helical fields, see e.g. [50].
- *Axion-induced UV cascade of helical electromagnetic fields.* Our simple estimates suggest that an axion induces helical electromagnetic fields to undergo a UV cascade, when the condition (2.17) is satisfied. If true, this would provide an absolute upper bound on the amplitude of large-scale helical electromagnetic fields in our universe, in terms of the axion coupling. It is also important to understand the axion abundance in this cascading regime.

⁷The misalignment scenario with late reheating is discussed in [47–49]. We should also note that the evolution of the conductivity depends not only on the reheating temperature, but also on the details of the reheating process.

- *Further imprints.* In addition to affecting the axion field dynamics, primordial (hidden) electromagnetic fields can induce conversions between axions and (hidden) photons [51, 52]. The helical electromagnetic background can also leave parity-violating signatures in cosmological observations (see e.g. [53] for signals from helical SM magnetic fields). It will be interesting to systematically analyze the range of signals arising in a universe with axions and primordial electromagnetic fields.

The effects listed here can provide us with further opportunities to probe the interplay between axions and primordial electromagnetic fields. We leave a detailed study of them to future work.

Acknowledgments

We thank Martin Sloth and Lorenzo Ubaldi for useful comments on a draft of this paper, and Kiyotomo Ichiki and Hiroyuki Tashiro for helpful discussions. RKJ would like to acknowledge financial support from the new faculty seed start-up grant of IISc, the Core Research Grant CRG/2018/002200 from the Science and Engineering Research Board, Department of Science and Technology, Government of India and the Infosys Foundation, Bangalore.

A Early Cosmological Evolution of Helical Electromagnetic Fields

We study the cosmological evolution of helical electromagnetic fields that have been produced in the early universe, and show that they do not necessarily redshift in a radiation-like manner in a vacuum as one would naively expect. The discussion here closely follows the work [54].

A.1 Model with a Time-Dependent and Parity-Violating Background

In this appendix we assume the helical electromagnetic fields to arise from a background that spontaneously breaks time diffeomorphisms as well as parity. As a simple toy example, we study the following U(1) gauge field theory,

$$S = \frac{1}{4} \int d^4x \sqrt{-g} \left[-I(\tau)^2 F_{\mu\nu} F^{\mu\nu} + J(\tau) F_{\mu\nu} \tilde{F}^{\mu\nu} \right]. \quad (\text{A.1})$$

The dual field strength is defined as in (2.2), and we fix the metric to a flat FRW, $ds^2 = a(\tau)^2(-d\tau^2 + d\mathbf{x}^2)$. The explicit time dependence of the coefficients I and J are understood to arise from couplings to other coherent degrees of freedom, such as a time-evolving scalar (see e.g. [7, 8, 10–14, 55, 56] for explicit models). These time-dependent coefficients violate the Weyl invariance of the Yang–Mills action and enables the production of electromagnetic fields in a Weyl-flat spacetime. The term $J(\tau)F\tilde{F}$ further violates parity and thus allows the fields to be helical.⁸ $I(\tau)^2$ is assumed to be positive definite.

⁸A general gauge field theory with spontaneously broken time diffeomorphisms can further include terms such as $\mathcal{K}(\tau)F^0{}_{\mu}F^{0\mu}$, which yields a variable speed of light [57]. However the model of (A.1) is good enough for our purpose of studying the redshifting behaviors of electromagnetic fields after they are produced.

The spatial components of the gauge field can be decomposed into irrotational and incompressible parts,

$$A_\mu = (A_0, \partial_i S + V_i) \quad \text{with} \quad \partial_i V_i = 0, \quad (\text{A.2})$$

where a sum over repeated spatial indices is implied irrespective of their positions. Noting that A_0 is a Lagrange multiplier whose constraint equation under proper boundary conditions gives $A_0 = S'$ (a prime denotes a derivative with respect to the conformal time τ), one can eliminate both A_0 and S from the action to yield, up to surface terms,

$$S = \frac{1}{2} \int d\tau d^3x \left[I^2 (V'_i V'_i - \partial_i V_j \partial_i V_j) - J' \epsilon_{0ijl} V_i \partial_j V_l \right]. \quad (\text{A.3})$$

Here we have written the totally antisymmetric pseudotensor as $\eta_{\mu\nu\rho\sigma} = -\sqrt{-g}\epsilon_{\mu\nu\rho\sigma}$ using a Levi-Civita symbol with $|\epsilon_{0123}| = 1$ and $\epsilon_{0123} = \epsilon^{0123}$.

We introduce two orthonormal polarization vectors $e_i^1(\mathbf{k})$ and $e_i^2(\mathbf{k})$ that satisfy

$$e_i^p(\mathbf{k}) k_i = 0, \quad e_i^p(\mathbf{k}) e_i^q(\mathbf{k}) = \delta^{pq}, \quad \text{for } p, q = \{1, 2\}, \quad (\text{A.4})$$

and their combinations,

$$e_i^\pm(\mathbf{k}) = \frac{1}{\sqrt{2}} (e_i^1(\mathbf{k}) \pm i e_i^2(\mathbf{k})). \quad (\text{A.5})$$

It can be checked that these vectors satisfy

$$e_i^+(\mathbf{k}) e_j^-(\mathbf{k}) + e_i^-(\mathbf{k}) e_j^+(\mathbf{k}) = \delta_{ij} - \frac{k_i k_j}{k^2}, \quad \epsilon_{0ijl} k_j e_l^\pm(\mathbf{k}) = \mp i k e_i^\pm(\mathbf{k}). \quad (\text{A.6})$$

Here $k \equiv \sqrt{k_i k_i}$, and we have chosen the directions of the polarization vectors such that the signs in the right hand side of the second equation are as shown. We further require the polarization vectors to satisfy

$$e_i^1(\mathbf{k})^* = e_i^1(\mathbf{k}), \quad e_i^2(\mathbf{k})^* = e_i^2(\mathbf{k}), \quad e_i^1(-\mathbf{k}) = e_i^1(\mathbf{k}), \quad e_i^2(-\mathbf{k}) = -e_i^2(\mathbf{k}), \quad (\text{A.7})$$

so that

$$e_i^\pm(\mathbf{k})^* = e_i^\mp(\mathbf{k}), \quad e_i^\pm(-\mathbf{k}) = e_i^\mp(\mathbf{k}). \quad (\text{A.8})$$

A.2 Canonical Quantization

We now quantize the gauge field by promoting V_i to an operator,

$$V_i(\tau, \mathbf{x}) = \int \frac{d^3k}{(2\pi)^3} \left[e_i^+(\mathbf{k}) \left\{ e^{i\mathbf{k}\cdot\mathbf{x}} a_{\mathbf{k}} u_{\mathbf{k}}^+(\tau) + e^{-i\mathbf{k}\cdot\mathbf{x}} b_{\mathbf{k}}^\dagger u_{\mathbf{k}}^-(\tau)^* \right\} \right. \\ \left. + e_i^-(\mathbf{k}) \left\{ e^{i\mathbf{k}\cdot\mathbf{x}} b_{\mathbf{k}} u_{\mathbf{k}}^-(\tau) + e^{-i\mathbf{k}\cdot\mathbf{x}} a_{\mathbf{k}}^\dagger u_{\mathbf{k}}^+(\tau)^* \right\} \right], \quad (\text{A.9})$$

where we take the mode functions $u_{\mathbf{k}}^\pm(\tau)$ to obey the equations of motion,

$$u_{\mathbf{k}}^{\pm''} + 2\frac{I'}{I} u_{\mathbf{k}}^{\pm'} + \left(k^2 \pm \frac{J'}{I^2} k \right) u_{\mathbf{k}}^\pm = 0, \quad (\text{A.10})$$

and the time-independent annihilation and creation operators to have the commutation relations,

$$\begin{aligned} [a_{\mathbf{k}}, a_{\mathbf{q}}^\dagger] &= [b_{\mathbf{k}}, b_{\mathbf{q}}^\dagger] = (2\pi)^3 \delta^{(3)}(\mathbf{k} - \mathbf{q}), \\ [a_{\mathbf{k}}, a_{\mathbf{q}}] &= [b_{\mathbf{k}}, b_{\mathbf{q}}] = [a_{\mathbf{k}}, b_{\mathbf{q}}] = [a_{\mathbf{k}}, b_{\mathbf{q}}^\dagger] = \dots = 0. \end{aligned} \quad (\text{A.11})$$

We also take V_i and its conjugate momentum obtained from the action $S = \int d\tau d^3x \mathcal{L}$ as $\Pi_i = \partial\mathcal{L}/\partial V_i' = I^2 V_i'$, to obey the equal-time commutation relations

$$\begin{aligned} [V_i(\tau, \mathbf{x}), \Pi_j(\tau, \mathbf{y})] &= i \int \frac{d^3k}{(2\pi)^3} e^{i\mathbf{k}\cdot(\mathbf{x}-\mathbf{y})} \left(\delta_{ij} - \frac{k_i k_j}{k^2} \right), \\ [V_i(\tau, \mathbf{x}), V_j(\tau, \mathbf{y})] &= [\Pi_i(\tau, \mathbf{x}), \Pi_j(\tau, \mathbf{y})] = 0. \end{aligned} \quad (\text{A.12})$$

The two set of commutation relations are consistent with each other when the mode functions are independent of the direction of \mathbf{k} , i.e., $u_{\mathbf{k}}^\pm = u_{\mathbf{k}}^\pm$, and obey the normalization condition

$$I^2 (u_{\mathbf{k}}^\pm u_{\mathbf{k}}^{\pm'*} - u_{\mathbf{k}}^{\pm*} u_{\mathbf{k}}^{\pm'}) = i. \quad (\text{A.13})$$

Then, defining the vacuum state by $a_{\mathbf{k}}|0\rangle = b_{\mathbf{k}}|0\rangle = 0$ for $\forall \mathbf{k}$, we can compute the correlation functions of the electromagnetic fields (2.7),

$$\langle 0|X_\mu(\tau, \mathbf{x})Y^\mu(\tau, \mathbf{y})|0\rangle = \int \frac{d^3k}{4\pi k^3} e^{i\mathbf{k}\cdot(\mathbf{x}-\mathbf{y})} \mathcal{P}_{XY}(\tau, k), \quad \text{where } X, Y = \{E, B\}. \quad (\text{A.14})$$

The power spectrum for each combination of the fields are given in terms of the mode functions as

$$\mathcal{P}_{EE} = \frac{k^3}{2\pi^2 a^4} \sum_{p=\pm} |u_k^{p'}|^2, \quad \mathcal{P}_{BB} = \frac{k^5}{2\pi^2 a^4} \sum_{p=\pm} |u_k^p|^2, \quad \mathcal{P}_{EB} = \frac{k^4}{4\pi^2 a^4} (|u_k^-|^2 - |u_k^+|^2)'. \quad (\text{A.15})$$

We thus clearly see that a correlation between the electric and magnetic fields \mathcal{P}_{EB} reflects an asymmetry between the two helicity modes. If the two modes start from the same initial condition (vacuum), then the difference can arise only from the difference in their time evolutions, which is sourced by the time dependence of J , as seen in the equation of motion (A.10).

A.3 Redshifting of Electromagnetic Fields within Maxwell Theory

Let us assume that after the helical electromagnetic fields have been produced by the time-varying I and J , the coefficients approach $I^2 = 1$ and $J' = 0$, recovering the standard Maxwell theory. Then the mode functions reduce to a sum of plane waves,

$$u_{\mathbf{k}}^\pm = \frac{1}{\sqrt{2k}} \left(\alpha_{\mathbf{k}}^\pm e^{-ik\tau} + \beta_{\mathbf{k}}^\pm e^{ik\tau} \right), \quad (\text{A.16})$$

where $\alpha_{\mathbf{k}}^\pm$ and $\beta_{\mathbf{k}}^\pm$ are time-independent complex numbers satisfying $|\alpha_{\mathbf{k}}^\pm|^2 - |\beta_{\mathbf{k}}^\pm|^2 = 1$ as required by the normalization condition (A.13). Note that $|\beta_{\mathbf{k}}^\pm|^2$ corresponds to the number of photons with polarization \pm , per six-dimensional comoving phase volume. Thus we have

$$\begin{aligned} |u_{\mathbf{k}}^\pm|^2 &= \frac{1}{2k} \left[1 + 2|\beta_{\mathbf{k}}^\pm|^2 + 2|\beta_{\mathbf{k}}^\pm| \sqrt{1 + |\beta_{\mathbf{k}}^\pm|^2} \cos \{ \arg(\alpha_{\mathbf{k}}^\pm \beta_{\mathbf{k}}^{\pm*}) - 2k\tau \} \right], \\ |u_{\mathbf{k}}^{\pm'}|^2 &= \frac{k}{2} \left[1 + 2|\beta_{\mathbf{k}}^\pm|^2 - 2|\beta_{\mathbf{k}}^\pm| \sqrt{1 + |\beta_{\mathbf{k}}^\pm|^2} \cos \{ \arg(\alpha_{\mathbf{k}}^\pm \beta_{\mathbf{k}}^{\pm*}) - 2k\tau \} \right], \\ (|u_{\mathbf{k}}^\pm|^2)' &= 2|\beta_{\mathbf{k}}^\pm| \sqrt{1 + |\beta_{\mathbf{k}}^\pm|^2} \sin \{ \arg(\alpha_{\mathbf{k}}^\pm \beta_{\mathbf{k}}^{\pm*}) - 2k\tau \}, \end{aligned} \quad (\text{A.17})$$

with which the power spectra of the electromagnetic fields (A.15) can be evaluated.⁹ The explicit values of the constants $|\beta_k^\pm|$ and $\arg(\alpha_k^\pm \beta_k^{\pm*})$ depend on the gauge field-producing model described by $I(\tau)$ and $J(\tau)$. Below we present two brief case studies where the electromagnetic correlators redshift in radiation-like and non-radiation-like manners, respectively.

Radiation-like Redshifting

Suppose that the $+$ mode has been exclusively produced so that $|\beta_k^+|^2 \gg |\beta_k^-|^2, 1$. Further assuming that the phase $\{\arg(\alpha_k^+ \beta_k^{+*}) - 2k\tau\}$ is not close to $n\pi$ ($n = 0, \pm 1, \pm 2, \dots$) such that the leading terms in the expressions of (A.17) do not cancel each other or vanish, then we see that the magnitudes of the three types of correlators are all of the same order,

$$\mathcal{P}_{EE} \sim \mathcal{P}_{BB} \sim |\mathcal{P}_{EB}| \sim \frac{k^4}{a^4} |\beta_k^+|^2. \quad (\text{A.18})$$

In this case, all power spectra exhibit a radiation-like redshifting of $\mathcal{P}_{XY} \propto a^{-4}$.

Non-Radiation-like Redshifting

For the second case, we expand the phase around π as

$$\arg(\alpha_k^\pm \beta_k^{\pm*}) - 2k\tau \equiv \pi + \theta_k^\pm, \quad (\text{A.19})$$

and suppose that this phase parameter and photon density satisfy the following relations,

$$\frac{1}{|\beta_k^\pm|^2} \ll |\theta_k^\pm| \ll 1, \quad |\theta_k^-|^n |\beta_k^-|^2 \ll |\theta_k^+|^n |\beta_k^+|^2 \quad \text{for } n = 0, 1, 2. \quad (\text{A.20})$$

It then follows that the power spectra are approximated by

$$\mathcal{P}_{EE} \simeq \frac{k^4}{\pi^2 a^4} |\beta_k^+|^2, \quad \mathcal{P}_{BB} \simeq \frac{k^4}{4\pi^2 a^4} (\theta_k^+)^2 |\beta_k^+|^2, \quad \mathcal{P}_{EB} \simeq \frac{k^4}{2\pi^2 a^4} \theta_k^+ |\beta_k^+|^2, \quad (\text{A.21})$$

which entails a hierarchy $\mathcal{P}_{EE} \gg |\mathcal{P}_{EB}| \gg \mathcal{P}_{BB}$. (The case with an inverted hierarchy $\mathcal{P}_{EE} \ll |\mathcal{P}_{EB}| \ll \mathcal{P}_{BB}$ can be realized under $\arg(\alpha_k^\pm \beta_k^{\pm*}) - 2k\tau \approx 0$.)

Now, considering that the conformal time in an FRW universe typically scales as $\tau \sim (aH)^{-1} + \text{const.}$ with $H = a'/a^2$ being the Hubble rate, let us suppose the phase parameter to evolve in time as $\theta_k^+ \propto (aH)^{-1}$. Then it follows that the power spectra redshift as

$$\mathcal{P}_{EE} \propto \frac{1}{a^4}, \quad \mathcal{P}_{BB} \propto \frac{1}{a^6 H^2}, \quad \mathcal{P}_{EB} \propto \frac{1}{a^5 H}. \quad (\text{A.22})$$

Thus in a decelerating universe, the BB and EB power redshift slower than a^{-4} . These scaling behaviors can also be understood from Faraday's law of induction. For further discussions on this point, and also for explicit models that produce electromagnetic fields with such non-radiation-like scalings, the reader is referred to [54].

⁹Using (A.17) one also obtains $\langle \rho_A \rangle = \langle E_\mu E^\mu + B_\mu B^\mu \rangle / 2 > |\langle E_\mu B^\mu \rangle|$ by evaluating the correlation functions at a single spacetime point. This inequality is slightly different from (2.8) due to the zero-point fluctuations, however we remark that this computation is too naive and a more rigorous treatment in the coincidence limit [58] would be necessary for discussing this inequality relation at the quantum level.

References

- [1] S. Weinberg, *A New Light Boson?*, *Phys. Rev. Lett.* **40** (1978) 223.
- [2] F. Wilczek, *Problem of Strong P and T Invariance in the Presence of Instantons*, *Phys. Rev. Lett.* **40** (1978) 279.
- [3] R. D. Peccei and H. R. Quinn, *CP Conservation in the Presence of Instantons*, *Phys. Rev. Lett.* **38** (1977) 1440.
- [4] P. Svrcek and E. Witten, *Axions In String Theory*, *JHEP* **06** (2006) 051 [[hep-th/0605206](#)].
- [5] M. R. Douglas and S. Kachru, *Flux compactification*, *Rev. Mod. Phys.* **79** (2007) 733 [[hep-th/0610102](#)].
- [6] A. Arvanitaki, S. Dimopoulos, S. Dubovsky, N. Kaloper and J. March-Russell, *String Axiverse*, *Phys. Rev.* **D81** (2010) 123530 [[0905.4720](#)].
- [7] M. S. Turner and L. M. Widrow, *Inflation Produced, Large Scale Magnetic Fields*, *Phys. Rev.* **D37** (1988) 2743.
- [8] B. Ratra, *Cosmological 'seed' magnetic field from inflation*, *Astrophys. J.* **391** (1992) L1.
- [9] K. Subramanian, *The origin, evolution and signatures of primordial magnetic fields*, *Rept. Prog. Phys.* **79** (2016) 076901 [[1504.02311](#)].
- [10] W. Garretson, G. B. Field and S. M. Carroll, *Primordial magnetic fields from pseudoGoldstone bosons*, *Phys. Rev. D* **46** (1992) 5346 [[hep-ph/9209238](#)].
- [11] M. M. Anber and L. Sorbo, *N-flationary magnetic fields*, *JCAP* **0610** (2006) 018 [[astro-ph/0606534](#)].
- [12] R. Durrer, L. Hollenstein and R. K. Jain, *Can slow roll inflation induce relevant helical magnetic fields?*, *JCAP* **1103** (2011) 037 [[1005.5322](#)].
- [13] C. T. Byrnes, L. Hollenstein, R. K. Jain and F. R. Urban, *Resonant magnetic fields from inflation*, *JCAP* **03** (2012) 009 [[1111.2030](#)].
- [14] P. Adshead, J. T. Giblin, T. R. Scully and E. I. Sfakianakis, *Magnetogenesis from axion inflation*, *JCAP* **10** (2016) 039 [[1606.08474](#)].
- [15] L. Campanelli and M. Giannotti, *Production of axions by cosmic magnetic helicity*, *Phys. Rev. Lett.* **96** (2006) 161302 [[astro-ph/0512458](#)].
- [16] A. J. Long and T. Vachaspati, *Implications of a Primordial Magnetic Field for Magnetic Monopoles, Axions, and Dirac Neutrinos*, *Phys. Rev. D* **91** (2015) 103522 [[1504.03319](#)].
- [17] M. Dvornikov and V. Semikoz, *Evolution of axions in the presence of primordial magnetic fields*, [2011.12712](#).

- [18] K. Choi and S. H. Im, *Realizing the relaxation from multiple axions and its UV completion with high scale supersymmetry*, *JHEP* **01** (2016) 149 [[1511.00132](#)].
- [19] D. E. Kaplan and R. Rattazzi, *Large field excursions and approximate discrete symmetries from a clockwork axion*, *Phys. Rev. D* **93** (2016) 085007 [[1511.01827](#)].
- [20] A. De Simone, T. Kobayashi and S. Liberati, *Geometric Baryogenesis from Shift Symmetry*, *Phys. Rev. Lett.* **118** (2017) 131101 [[1612.04824](#)].
- [21] T. Kobayashi and L. Ubaldi, *Inflation Dark Matter*, *JHEP* **08** (2019) 147 [[1907.00984](#)].
- [22] T. Kobayashi and L. Ubaldi, *Reheating-Induced Axion Dark Matter After Low Scale Inflation*, *JHEP* **09** (2020) 052 [[2006.09389](#)].
- [23] M. Kamionkowski and J. March-Russell, *Planck scale physics and the Peccei-Quinn mechanism*, *Phys. Lett. B* **282** (1992) 137 [[hep-th/9202003](#)].
- [24] R. Holman, S. D. Hsu, T. W. Kephart, E. W. Kolb, R. Watkins and L. M. Widrow, *Solutions to the strong CP problem in a world with gravity*, *Phys. Lett. B* **282** (1992) 132 [[hep-ph/9203206](#)].
- [25] R. T. Co, L. J. Hall and K. Harigaya, *Axion Kinetic Misalignment Mechanism*, *Phys. Rev. Lett.* **124** (2020) 251802 [[1910.14152](#)].
- [26] J. Preskill, M. B. Wise and F. Wilczek, *Cosmology of the Invisible Axion*, *Phys. Lett. B* **120** (1983) 127.
- [27] L. Abbott and P. Sikivie, *A Cosmological Bound on the Invisible Axion*, *Phys. Lett. B* **120** (1983) 133.
- [28] M. Dine and W. Fischler, *The Not So Harmless Axion*, *Phys. Lett. B* **120** (1983) 137.
- [29] L. Kofman, A. D. Linde and A. A. Starobinsky, *Towards the theory of reheating after inflation*, *Phys. Rev. D* **56** (1997) 3258 [[hep-ph/9704452](#)].
- [30] PLANCK collaboration, *Planck 2018 results. VI. Cosmological parameters*, *Astron. Astrophys.* **641** (2020) A6 [[1807.06209](#)].
- [31] R. Z. Ferreira and M. S. Sloth, *Universal Constraints on Axions from Inflation*, *JHEP* **12** (2014) 139 [[1409.5799](#)].
- [32] R. Z. Ferreira, J. Ganc, J. Noreña and M. S. Sloth, *On the validity of the perturbative description of axions during inflation*, *JCAP* **04** (2016) 039 [[1512.06116](#)].
- [33] P. Agrawal, G. Marques-Tavares and W. Xue, *Opening up the QCD axion window*, *JHEP* **03** (2018) 049 [[1708.05008](#)].
- [34] N. Kitajima, T. Sekiguchi and F. Takahashi, *Cosmological abundance of the QCD axion coupled to hidden photons*, *Phys. Lett. B* **781** (2018) 684 [[1711.06590](#)].

- [35] M. S. Turner, *Cosmic and Local Mass Density of Invisible Axions*, *Phys. Rev.* **D33** (1986) 889.
- [36] K. J. Bae, J.-H. Huh and J. E. Kim, *Update of axion CDM energy*, *JCAP* **0809** (2008) 005 [[0806.0497](#)].
- [37] L. Hui, J. P. Ostriker, S. Tremaine and E. Witten, *Ultralight scalars as cosmological dark matter*, *Phys. Rev.* **D95** (2017) 043541 [[1610.08297](#)].
- [38] W. Hu, R. Barkana and A. Gruzinov, *Cold and fuzzy dark matter*, *Phys. Rev. Lett.* **85** (2000) 1158 [[astro-ph/0003365](#)].
- [39] V. Iršič, M. Viel, M. G. Haehnelt, J. S. Bolton and G. D. Becker, *First constraints on fuzzy dark matter from Lyman- α forest data and hydrodynamical simulations*, *Phys. Rev. Lett.* **119** (2017) 031302 [[1703.04683](#)].
- [40] E. Armengaud, N. Palanque-Delabrouille, C. Yèche, D. J. E. Marsh and J. Baur, *Constraining the mass of light bosonic dark matter using SDSS Lyman- α forest*, *Mon. Not. Roy. Astron. Soc.* **471** (2017) 4606 [[1703.09126](#)].
- [41] T. Kobayashi, R. Murgia, A. De Simone, V. Iršič and M. Viel, *Lyman- α constraints on ultralight scalar dark matter: Implications for the early and late universe*, *Phys. Rev.* **D96** (2017) 123514 [[1708.00015](#)].
- [42] N. Bar, D. Blas, K. Blum and S. Sibiryakov, *Galactic rotation curves versus ultralight dark matter: Implications of the soliton-host halo relation*, *Phys. Rev.* **D98** (2018) 083027 [[1805.00122](#)].
- [43] G. Grilli di Cortona, E. Hardy, J. Pardo Vega and G. Villadoro, *The QCD axion, precisely*, *JHEP* **01** (2016) 034 [[1511.02867](#)].
- [44] S. Borsanyi et al., *Calculation of the axion mass based on high-temperature lattice quantum chromodynamics*, *Nature* **539** (2016) 69 [[1606.07494](#)].
- [45] PARTICLE DATA GROUP collaboration, *Review of Particle Physics*, *PTEP* **2020** (2020) 083C01.
- [46] T. Kobayashi, R. Kurematsu and F. Takahashi, *Isocurvature Constraints and Anharmonic Effects on QCD Axion Dark Matter*, *JCAP* **1309** (2013) 032 [[1304.0922](#)].
- [47] G. Lazarides, C. Panagiotakopoulos and Q. Shafi, *Relaxing the Cosmological Bound on Axions*, *Phys. Lett.* **B192** (1987) 323.
- [48] T. Banks and M. Dine, *The Cosmology of string theoretic axions*, *Nucl. Phys.* **B505** (1997) 445 [[hep-th/9608197](#)].
- [49] G. F. Giudice, E. W. Kolb and A. Riotto, *Largest temperature of the radiation era and its cosmological implications*, *Phys. Rev.* **D64** (2001) 023508 [[hep-ph/0005123](#)].

- [50] T. Fujita and R. Durrer, *Scale-invariant Helical Magnetic Fields from Inflation*, *JCAP* **09** (2019) 008 [[1904.11428](#)].
- [51] P. Sikivie, *Experimental Tests of the Invisible Axion*, *Phys. Rev. Lett.* **51** (1983) 1415.
- [52] K. Kamada and Y. Nakai, *Axion production from primordial magnetic fields*, *Phys. Rev. D* **96** (2017) 023537 [[1702.03928](#)].
- [53] L. Pogosian, T. Vachaspati and S. Winitzki, *Signatures of kinetic and magnetic helicity in the CMBR*, *Phys. Rev. D* **65** (2002) 083502 [[astro-ph/0112536](#)].
- [54] T. Kobayashi and M. S. Sloth, *Early Cosmological Evolution of Primordial Electromagnetic Fields*, *Phys. Rev. D* **100** (2019) 023524 [[1903.02561](#)].
- [55] R. J. Ferreira, R. K. Jain and M. S. Sloth, *Inflationary magnetogenesis without the strong coupling problem*, *JCAP* **10** (2013) 004 [[1305.7151](#)].
- [56] R. J. Z. Ferreira, R. K. Jain and M. S. Sloth, *Inflationary Magnetogenesis without the Strong Coupling Problem II: Constraints from CMB anisotropies and B-modes*, *JCAP* **1406** (2014) 053 [[1403.5516](#)].
- [57] D. Green and T. Kobayashi, *Constraints on Primordial Magnetic Fields from Inflation*, *JCAP* **1603** (2016) 010 [[1511.08793](#)].
- [58] N. D. Birrell and P. C. W. Davies, *Quantum Fields in Curved Space*, Cambridge Monographs on Mathematical Physics. Cambridge University Press, 1982.